

Effect of Current Pulsation on Weld Microstructure During Micro-Plasma Arc Welding of Inconel 718



A. K. Sahu  and Swarup Bag 

1 Introduction

Superalloy 718 (also known as Inconel 718) is the most widely recognized Ni–Fe-based alloy which exhibits excellent mechanical and oxidation resistance property up to the temperature of 650 °C [1]. Hence, the alloy is found to be desirable for numerous high-temperature applications even in the extreme environments, such as gas turbine disks, casings, shafts, and liners in aerospace and nuclear power generation industries. The superalloy shows exceptional fusion welding quality owing to the sluggish precipitation of alloy's principal strengthening phase γ'' (BCT, Ni₃Nb), which provides resistance to strain age cracking and solidification cracking [2, 3]. The primary challenge involved with the fabrication of superalloy 718 is the segregation of Niobium in the interdendritic zone and precipitation of various secondary phases (i.e., NbC and Laves) which promotes the microfissuring or liquation cracks in the heat-affected and fusion zone (FZ) [4–7]. Hence, the presence of Laves phase which is a Nb enriched intermetallic phase (represented as, Fe₂Nb) in the interdendritic zones during solidification has deleterious impact on the mechanical properties like tensile strength, hardness, ductility, fatigue, and creep rupture strength [1, 8]. Precipitation of Laves and different carbides not merely provides micro-crack initiation sites in the FZ and HAZ but also consume a substantial amount of favorable strengthening alloying elements out of the metal matrix.

Laves phase is an unavoidable intermetallic phase present mainly in the interdendritic region of fusion welded component [9]. Hence, reduction in volume percentage of Laves phase by using various advanced welding technique has resulted in weld quality improvement. The amount of heat input (J/mm) during

A. K. Sahu (✉) · S. Bag

Department of Mechanical Engineering, Indian Institute of Technology Guwahati, Guwahati, Assam 781039, India

e-mail: ajit.sahu@iitg.ac.in

welding plays a pivotal role for amount of segregation and precipitation of Laves phase. Low heat input during welding assures a steep thermal gradient during solidification of weld pool which hinders the segregation tendency of the solutes like Nb, Mo, and Ti in the interdendritic zones and leads to a refined microstructure in the weld zone. Many studies have focused on various advanced welding techniques like laser beam welding (LBW) and electron beam welding (EBM) to achieve low heat input and high cooling rate to control the segregation tendency and to further improve the mechanical strength of Inconel 718 welded structure [1, 2, 10]. Apart from the heat input, techniques like current pulsation and beam oscillation were also used to control the Nb segregation and Laves phase formation [10–12]. The application of current pulsation during welding concludes in remarkable grain refinement of the solidified structure. The microstructure refinement during solidification occurs mainly due to the periodic change in the weld pool temperature. The cyclic temperature variation enhances the fluid flow inside the weld pool and facilitates to break the long continuous chain of Laves particle during the solidification. Ram et al. [11] reported the application of current pulsation during GTA welding leads to contraction in Laves phase volume percentage and enhancement in the weld mechanical characteristics. Ram et al. [13] witnessed very fine and discrete weld morphology and lower segregation of principal alloying elements in the interdendritic region with the pulsed Nd-YAG laser welding as compared to the GTA welding technique. Radhakrishna and Rao [10] used electron beam (EB) with circular oscillation technique to weld the Inconel 718 and found significant reduction in segregation of Nb and Laves phase precipitation in the weld zone. Till date, very minimal work is available on arc welding of superalloy 718 with current pulsation mode as compared to LBW and EB advanced welding techniques. Hence, it is worthwhile in the current study to analyze the cost-efficient micro-plasma arc welding (μ PAW) in constant and pulsed current mode to weld the solution treated superalloy 718 sheets and highlight the possibility in reducing weld segregation and precipitation of Laves phase. The primary aim of the present work is to investigate the impact of current pulsation on microstructure and mechanical characteristics of the welded joints.

2 Experimental Details

As received superalloy 718 rolled sheets of 0.7 mm thickness are undergone solution treatments at 980 °C for 1 h followed by water quenching to obtain a homogeneous microstructure. The solution treated sheets are cut into 90 × 55 mm coupons, and the welding direction is kept in normal to the sheet rolling direction. In order to figure out the elemental composition (wt%), energy dispersive X-ray (EDX) investigation is conducted on the base material and the result is shown in Fig. 1a. In reference to the EDX probe, the parent material composition is presented in Table 1. The optical microstructure of superalloy 718 parent material is demonstrated in Fig. 1b. The base material wrought austenite consisting of

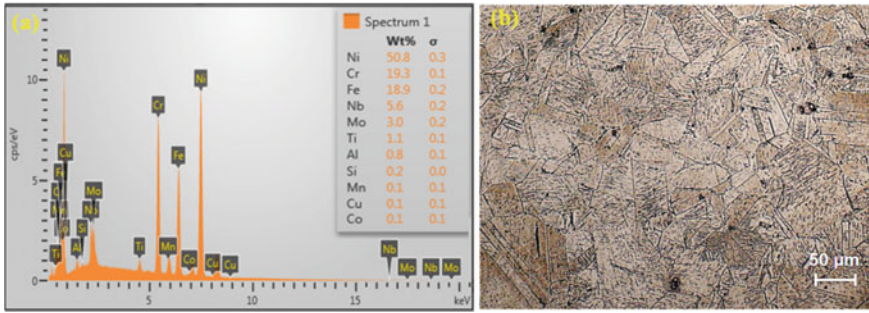


Fig. 1 Showing **a** EDX elemental analysis and **b** optical microstructure of the base material

Table 1 Chemical composition (wt%) of superalloy 718

Elements	Ni	Cr	Nb	Mo	Ti	Al
Composition (wt%)	50.8	19.3	5.6	3.0	1.1	0.8
Elements	Si	Mn	Cu	Co		Fe
Composition (wt%)	0.2	0.1	0.1	0.1		Bal.

equiaxed-type grains with an average grain diameter of 63 μm (ASTM 5–6) are observed in the micrograph. Discrete needle shape δ phase and randomly distributed MC (M: Nb, Ti) carbides are also evident in the microstructure. The welding surfaces are thoroughly cleaned before the welding process to remove the oxides and different impurities present on the surface. Sheets are tightened in a fixture made up of copper to curb the deformation and achieve high cooling rate throughout the welding process. The welding torch of micro-plasma setup is held stationary, and the workpiece is enabled to move with a consistent velocity. Commercial pure argon gas of 99% purity is employed as plasma gas in addition to shielding gas to cover the weld pool from atmosphere. Butt configured welded joints are produced through constant current (CC) and pulsed current (PC) method using a micro-plasma arc welding machine with DCEN power supply. The plasma and shielding gas flow speed are kept at 0.4 and 5 L/min, respectively, along with a nozzle standoff gap of 2 mm. The remaining welding variables adopted for producing defect less welds by constant and pulsed current conditions are presented in the Table 2, usually acquired by broad range of welding trials with keeping the heat input (J/mm) constant in both the condition.

The welded specimens are cut normal to the welding direction for microstructural analysis and polished with emery paper followed by velvet cloth polishing with the diamond paste (0.5–1 μm) to obtain mirror finish. The polished samples are dip for few seconds in a mixture of HCl, HF, and HNO₃ in the proportion of 4:2:1, respectively, to obtain the microstructure. The microstructural investigation is performed through the optical microscope and scanning electron microscope

Table 2 Welding parameters employed for CC (58.5 J/mm) and PC (59 J/mm) weld

<i>Constant current welding</i>	
Current, A	15
Welding speed, mm s ⁻¹	4
Voltage, V	24
<i>Pulse current welding</i>	
Peak current, A	18
Base current, A	5.4
Welding speed, mm s ⁻¹	4
Pulse frequency, Hz	6
Pulse-on time	30% of cycle time
Voltage, V	24

(SEM). The volume percentage of Laves intermetallic phase is evaluated through the image analysis technique on the SEM micrographs, taken from fusion boundary to weld center for both the welding conditions. X-ray diffraction (XRD) technique is carried out on CC and PC weld zone to reveal the composition and presence of various intermetallic phases along with the main austenite matrix. Micro-hardness measurements are conducted across the weld bead with an indentation spacing of 0.2 mm for each specimen, using Vickers hardness tester at a load of 500 g and a dwell time of 20 s. The hardness is evaluated in the center portion of the welded joint. Tensile testing of the welded samples and base material is undertaken at room temperature to analyze the proof stress, tensile strength, and degree of elongation. For every condition, three sub-size specimens are prepared according to usual ASTM E8M subsize standard. The tests are performed with a computer controlled servo-hydraulic universal tensile testing setup with extensometer attachment and a crosshead speed of 0.5 mm/min.

3 Results and Discussion

3.1 Microstructure

Figure 2 depicts the top and cross-sectional view of the weld bead obtained by CC and PC mode of welding. In both the cases, full penetration is achieved with a weld bead cap width of 1.9 mm and 2.7 mm and root width of 1.4 mm and 1.6 mm for CC and PC weld, respectively. Higher weld bead width in PC mode is owing to the increased heat input over the application of peak current (i.e., 18 A) during the pulse-on period as compared to CC mode of welding (i.e., 15 A). No significant difference in the weld surface geometry is observed except overlapped type weld pool due to the current pulsation in the PC mode as compared to wavy nature of weld pool in CC mode of welding is witnessed. From the optical microscopic

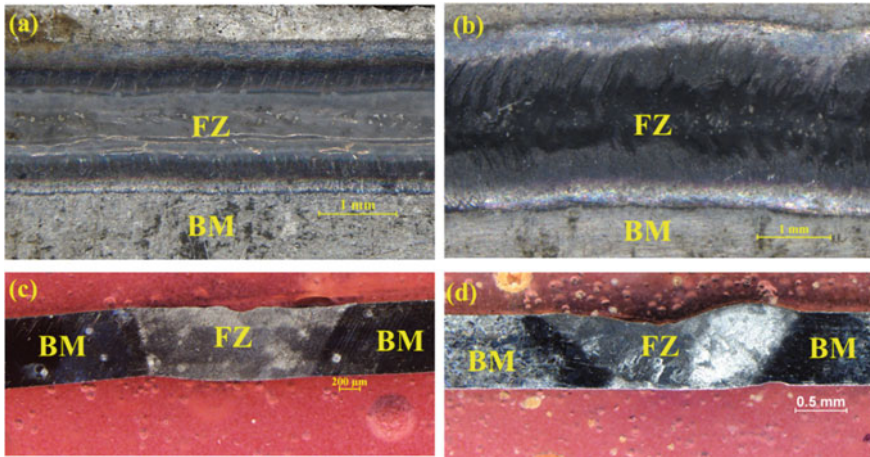


Fig. 2 Top and transverse view of weld bead produced by **a, c** constant current (CC) and **b, d** pulse current (PC) mode of welding

inspection, it is found that the acquired weld beads are independent from any kind of weld surface imperfections.

Figure 3 describes the microscopic view of weld fusion zone and fusion boundary for PC and CC conditions. Inconel 718 is a highly alloyed material; hence, the mode of solidification is of dendritic type. Columnar dendritic chain developed from the solid–liquid interface (fusion boundary) is seen in both the welding conditions. This is owing to the higher cooling rate near the fusion boundary [13]. The columnar dendritic growth near to the weld interface of PC weld results in fewer as compared to larger and continuous dendrites of CC weld, thus producing coarser and interconnected Laves particles in CC mode of welding [14]. The welds are observed to be free from microfissuring in the FZ and HAZ, and an extremely constricted heat-affected zone (HAZ) is witnessed in both the welding conditions.

The higher magnified micrographs of the weld interior reveal the mode of solidification dendrites for the PC and CC welds. The PC weld is witnessed to be fine and of equiaxed type, whereas the microstructure is observed to be coarser and columnar type for CC mode weld (Fig. 4). The variation in the fusion zone microstructural morphology is mainly due to the current pulsation effect during the welding [15, 16]. The solidification morphology depends upon the ratio of temperature gradient (G) and solidification growth rate (R). Lower value of (G/R) produces equiaxed dendritic structure. The current pulsation reduces thermal gradient in the weld pool by enhancing the fluid flow due to cyclic variation of temperature during the welding process [11]. In both the welding condition, solidification growth rate would be same due to equal welding speed [17]. Hence, at constant (R) reduction in (G) will reduce the (G/R) for the PC condition weld, resulting in equiaxed type of microstructure. Due to current pulsation, the cooling

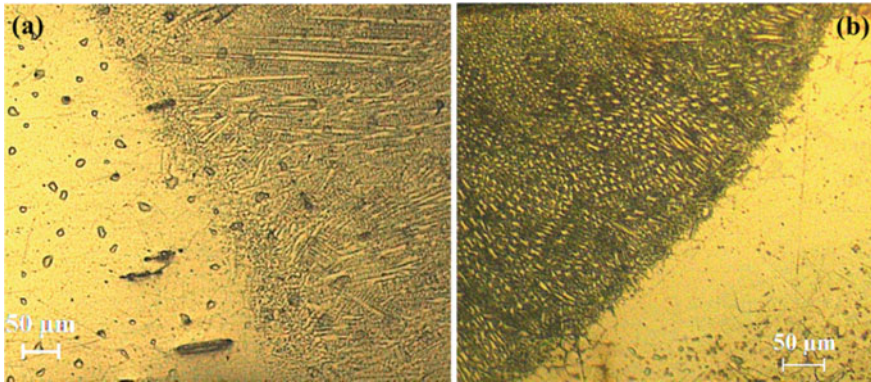


Fig. 3 Showing fusion boundary and heat affected zone of **a** CC and **b** PC welding condition

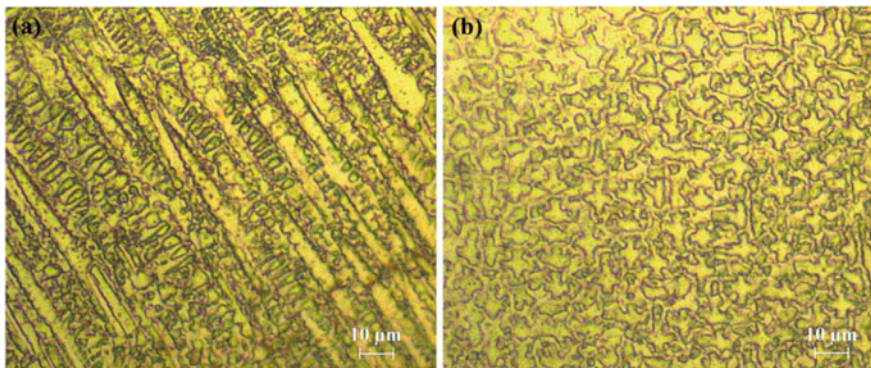


Fig. 4 Microstructure of the weld interior for **a** CC and **b** PC mode welding

rate also increases and results in decline of weld dendritic arm spacing and scale of the deleterious intermetallic phases [11].

The SEM analysis of the weld zone interior is shown in Fig. 5. At the weld interior, numbers of bright irregular-shaped Laves particles are observed in the interdendritic region. The Laves particles in CC weld are witnessed to be interconnect columnar type and moderately coarser against to the equiaxed dendrites of the PC weld. The current pulsation has refined the microstructure due to the temperature variation during the welding process. Through image analysis technique the average volume fraction (%) of interdendritic Laves phase in the weld interior is calculated as $15.5 \pm 1.3\%$ and $6.9 \pm 1.1\%$ for CC and PC weld, respectively. The continuous temperature variation during pulsed welding causes remelting and breaking off of the long continuous dendritic chain at the solidification front as a result reducing the segregation and volume percentage of intermetallic phase.

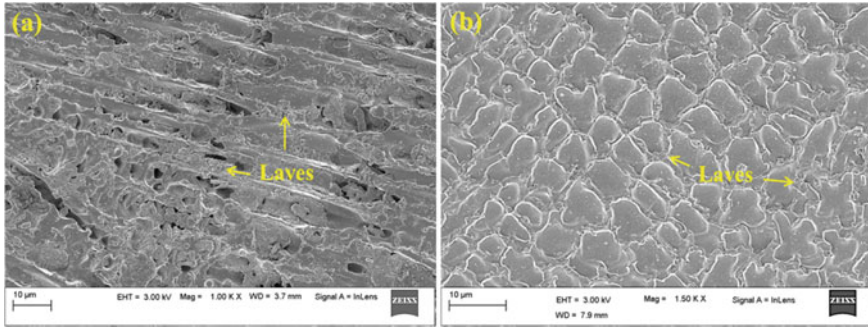


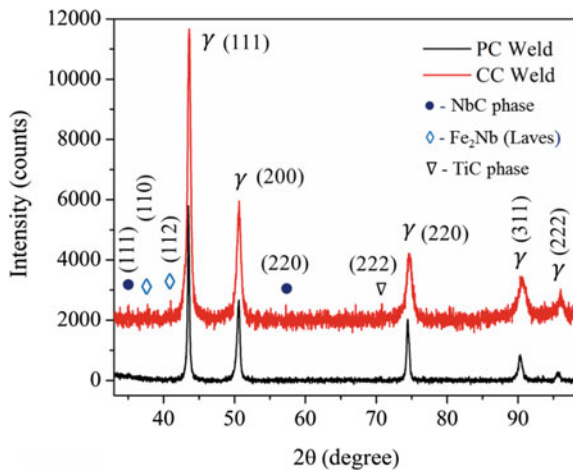
Fig. 5 SEM microstructure of weld interior for **a** CC mode and **b** PC mode weld

Hence, the amount (volume %) of Laves phase is higher in the columnar dendritic regions of CC weld as compared to the equiaxed dendrites of the PC mode weld [11].

3.2 XRD Analysis

The diffraction (XRD) peaks corresponding to the CC and PC weld zones are shown in Fig. 6. The main Fe–Ni austenite (γ) matrix dominating in (111) plane is witnessed from the sharp diffraction peak. The presence of diffraction peaks corresponding to various intermetallic phases such as Laves (Fe_2Nb), NbC, and TiC dominating in the direction (110) (112), (111) (220), and (222), respectively, are observed from the diffraction plot. The diffraction peaks corresponding to CC weld

Fig. 6 XRD analysis of the CC and PC weld zone



are found to be sharp and strong as compared to the peaks of PC weld. The small and weak peaks of PC weld will reduce the normalized intensity ratio (NIR) with respect to the CC weld, which signifies reduction in relative quantity of different intermetallic phases in the weld zone [18]. Hence, current pulsation during the welding hinders the precipitation of various secondary intermetallic phases in the solidified weld zone.

3.3 Mechanical Properties

The effect of segregation and formation of intermetallic phases on the weld mechanical properties are investigated. The micro-hardness test was carried out across the weld bead for both the cases, and the hardness profile is depicted in Fig. 7a. The base material hardness is found to be 215 ± 6 HV in the solution treated condition. The hardness of the CC weld falls in the fusion zone against the base material which is mainly due to segregation of principal strengthening alloying element. The development of intermetallic phases absorbs a substantial amount of principal alloying elements (i.e., Nb, Mo, and Ti) from the matrix, therefore reducing the hardness of the weld. The maximum fusion zone hardness in CC weld is found to be 206.2 HV. The presence of continuous Laves phase in the weld microstructure of CC weld, absorbs ample amount of Nb that were initially present in the base material, making accessible very less quantity of Nb for the precipitation of strengthening phases. For PC weld, the micro-hardness value is witnessed to be marginally higher than the CC weld zone. The maximum hardness of PC weld is found to be 222.2 HV. The hardness variation is primarily due to the refined microstructure of the PC fusion zone which leads to reduction of Laves phase formation, hence making ample amount of alloying element available in the metal matrix for the precipitation of strengthening phases. The hardness value of the HAZ drops in both the cases is attributed to the grain coarsening in the region due to generation of high temperature in the course of welding process.

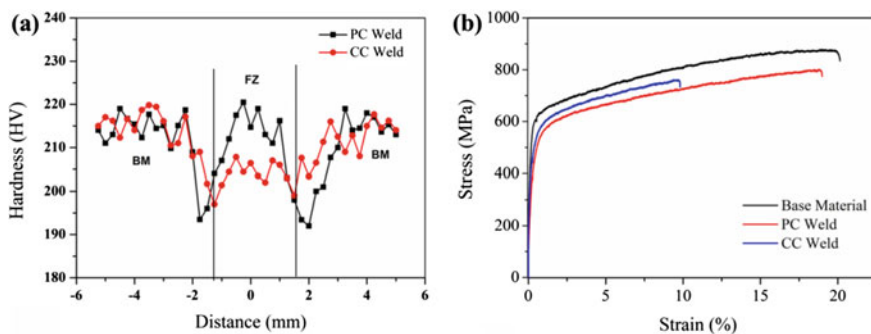


Fig. 7 a Microhardness distribution and b tensile strength of the base material and welded joints

Table 3 Tensile test results of welded samples

	Base material	PC weld metal	CC weld metal
Yield stress (MPa)	595 ± 11	485 ± 8	499 ± 10
UTS (MPa)	880 ± 13	803 ± 9	762 ± 11
Elongation, %	21.0 ± 1.1	19.0 ± 0.9	10.0 ± 0.8

The base material and weld metal tensile properties for PC and CC mode weld are given in Table 3, and the corresponding stress–strain plot is shown in Fig. 7b. The tensile strength of the base material is witnessed to be superior to both the CC and PC weld metals, and the properties of CC welds are found inferior to the PC weld material. All of the welded specimens are failed in the fusion zone area, hence making the FZ as the weakest region in the component due to the presence of intermetallic phases. The joint efficiency of the welded component with respect to the BM is found to be 91.2% and 86.5% for PC and CC condition, respectively. The differences in tensile characteristics are owing to the development of intermetallic Laves phase during the weld solidification. The Laves phase not just consumes essential alloying element from the metal matrix in addition also provides desirable location for crack initiation and growth in the fusion zone during the loading [13]. As a result, the tensile ductility of the CC weld is found to be less than 47% against the base material and around 52% of the PC weld. Hence, a significantly improvement in the tensile properties is witnessed by applying current pulsation during the welding process.

4 Conclusion

In the present work, micro-plasma arc welding of superalloy 718 in constant current (CC) and pulsed current (PC) mode has been undertaken and its effect on weld microstructure and mechanical behavior has been studied. The findings of the present work are as follows:

- Due to current pulsation, significant refinement of fusion zone microstructure is witnessed.
- In PC weld equiaxed dendrites are dominating in the weld interior, whereas in CC, columnar dendrites are dominating.
- Grain refinement and equiaxed dendrites reduce the amount of brittle intermetallic Laves phase more than 50% in the PC weld.
- Microstructural refinement due to current pulsing led to substantial enhancement in the micro-hardness and tensile characteristics of the welded joint.
- The tensile ductility improves by 47% by the application of current pulsation as compared to CC mode of welding.

Acknowledgements The authors are thankful to the department of Mechanical Engineering and Central Instrument Facility of IIT Guwahati for providing financial and experimental facilities to carry out the present study.

References

1. Radhakrishna C, Rao KP (1994) Studies on creep/stress rupture behaviour of superalloy 718 weldments used in gas turbine applications. *Mater High Temp* 12:323–327. <https://doi.org/10.1080/09603409.1994.11752536>
2. Gobbi S, Zhang L, Norris J, Richter KH, Loreau JH (1996) High powder CO₂ and Nd:YAG laser welding of wrought Inconel 718. *J Mater Process Technol* 56:333–345. [https://doi.org/10.1016/0924-0136\(95\)01847-6](https://doi.org/10.1016/0924-0136(95)01847-6)
3. Sahu AK, Bag S (2020) Effect of pre-weld solution treatment on mechanical properties and microstructure of micro-plasma arc welded Inconel 718. In: Shunmugam MS, Kanthababu M (eds) *Advances in additive manufacturing and joining*, pp 373–383. Springer, Singapore. https://doi.org/10.1007/978-981-32-9433-2_33
4. Thompson RG (1988) Microfissuring of alloy 718 in the weld heat-affected zone. *JOM* 40:44–48. <https://doi.org/10.1007/BF03258151>
5. Radhakrishnan B, Thompson RG (1992) A model for the formation and solidification of grain boundary liquid in the heat-affected zone (HAZ) of welds. *Metall Mat Trans A* 23:1783–1799. <https://doi.org/10.1007/BF02804371>
6. Cieslak MJ, Headley TJ, Knorovsky GA, Romig AD, Kollie T (1990) A comparison of the solidification behavior of INCOLOY 909 and INCONEL 718. *Metall Mat Trans A* 21:479–488. <https://doi.org/10.1007/BF02782428>
7. Sahu AK, Bag S (2019) Finite element modelling and experimental verification of dissimilar joining between Inconel 718 and SS 316L by micro-plasma arc welding. In: Narayanan RG, Joshi SN, Dixit US (eds) *Advances in computational methods in manufacturing*, pp 231–243. Springer, Singapore. https://doi.org/10.1007/978-981-32-9072-3_20
8. Hong JK, Park JH, Park NK, Eom IS, Kim MB, Kang CY (2008) Microstructures and mechanical properties of Inconel 718 welds by CO₂ laser welding. *J Mater Process Technol* 201:515–520. <https://doi.org/10.1016/j.jmatprotec.2007.11.224>
9. Cao X, Rivaux B, Jahazi M, Cuddy J, Birur A (2009) Effect of pre- and post-weld heat treatment on metallurgical and tensile properties of Inconel 718 alloy butt joints welded using 4 kW Nd:YAG laser. *J Mater Sci* 44:4557–4571. <https://doi.org/10.1007/s10853-009-3691-5>
10. Radhakrishna C, Prasad Rao K (1997) The formation and control of laves phase in superalloy 718 welds. *J Mater Sci* 32:1977–1984. <https://doi.org/10.1023/A:1018541915113>
11. Ram GDJ, Reddy AV, Rao KP, Reddy GM (2004) Control of laves phase in Inconel 718 GTA welds with current pulsing. *Sci Technol Weld Joining* 9:390–398. <https://doi.org/10.1179/136217104225021788>
12. Kumar B, Bag S, Paul CP, Das CR, Ravikumar R, Bindra KS (2020) Influence of the mode of laser welding parameters on microstructural morphology in thin sheet Ti6Al4V alloy. *Opt Laser Technol* 131:106456. <https://doi.org/10.1016/j.optlastec.2020.106456>
13. Janaki Ram GD, Venugopal Reddy A, Prasad Rao K, Reddy GM, Sarin Sundar JK (2005) Microstructure and tensile properties of Inconel 718 pulsed Nd-YAG laser welds. *J Mater Process Technol* 167:73–82. <https://doi.org/10.1016/j.jmatprotec.2004.09.081>
14. Sahu AK, Bag S, Huang K (2020) Mitigation of micro-cracks in dissimilar welding of Inconel 718 and austenitic stainless steel. *Philos Mag Lett* 0:1–10. <https://doi.org/10.1080/09500839.2020.1774674>
15. Ye X, Hua X, Wang M, Lou S (2015) Controlling hot cracking in Ni-based Inconel-718 superalloy cast sheets during tungsten inert gas welding. *J Mater Process Technol* 222:381–390. <https://doi.org/10.1016/j.jmatprotec.2015.03.031>

16. Sahu AK, Bag S (2020) Probe pulse conditions and solidification parameters for the dissimilar welding of Inconel 718 and AISI 316L stainless steel. *Metall Mat Trans A* 51:2192–2208. <https://doi.org/10.1007/s11661-020-05705-4>
17. Manikandan SGK, Sivakumar D, Rao KP, Kamaraj M (2014) Effect of weld cooling rate on laves phase formation in Inconel 718 fusion zone. *J Mater Process Technol* 214:358–364. <https://doi.org/10.1016/j.jmatprotec.2013.09.006>
18. Peelamedu RD, Roy R, Agrawal DK (2002) Microwave-induced reaction sintering of NiAl_2O_4 . *Mater Lett* 55:234–240. [https://doi.org/10.1016/S0167-577X\(01\)00653-X](https://doi.org/10.1016/S0167-577X(01)00653-X)